Biological versus physical processes as drivers of large oscillations of the air–sea CO_2 flux in the Antarctic marginal ice zone during summer

M.H.C. Stoll[a], H. Thomas[a,*], H.J.W. De Baar[a], I. Zondervan[b], E. De Jong[a], U.V. Bathmann[b], E. Fahrbach[b]

[a] *Department of Marine Chemistry and Geology, Royal Netherlands Institute for Sea Research, P.O. Box 59, NL-1790 AB Den Burg, Texel, The Netherlands*
[b] *Alfred Wegener Institute for Polar and Marine Research, P.O. Box 120161, D-27515 Bremerhaven, Germany*

Abstract

The fugacity of CO_2 and abundance of chlorophyll a (Chl$a$) were determined in two long transects from the Polar Front to the Antarctic Continent in austral summer, December 1995–January 1996. Large undersaturations of CO_2 in the surface water were observed coinciding with high Chl$a$ content. In the major hydrographic regions the mean air–sea fluxes were found to range from -3 to $+7\,mmol\,m^{-2}\,d^{-1}$ making these regions act as a sink as well as a source for CO_2. In the total 40-d period, the summation of the several strong source and sink regions revealed an overall modest net source of $0.3\,mmol\,m^{-2}\,d^{-1}$, this based on the Wanninkhof (J. Geophys. Res. 97 (1992) 7373) quadratic relationship at in situ windspeed. A simple budget approach was used to quantify the role of phytoplankton blooms in the inorganic carbonate system of the Antarctic seas in a time frame spanning several weeks. The major controlling physical factors such as air–sea flux, Ekman pumping and upwelling are included. Net community production varies between -9 and $+7\,mmol\,m^{-2}\,d^{-1}$, because of the large oscillations in the dominance of autotrophic (CO_2 fixation) versus heterotrophic (CO_2 respiration) activity. Here the mixed layer depth is the major controlling factor. When integrated over time the gross influx and efflux of CO_2 from air to sea is large, but the net residual air/sea exchange is a modest efflux from sea to atmosphere.

© 2002 Elsevier Science Ltd. All rights reserved.

Keywords: Antarctic front; CO_2 system; Total inorganic carbon; CO_2 partial pressure

1. Introduction

The strong increase in atmospheric concentrations of carbon dioxide (Keeling and Whorf, 1994) has generated considerable interest in the global carbon cycle (Sarmiento, 1993; Tans et al., 1990; Sarmiento et al., 1992). The oceans are thought to have taken up $\sim 1.9 \pm 0.6\,PgC\,a^{-1}$ from

*Corresponding author. Tel.: +31-222-369-438; fax: +31-222-319-674.
E-mail addresses: hthomas@nioz.nl (H. Thomas), efahrbach@awi-bremerhaven.de (E. Fahrbach).

anthropogenic sources (IPCC, 2001) during the 1980s and some high latitude areas exhibit the largest uptake rates. Later work reported a slightly lower number of $\sim 1.7\,\mathrm{PgC\,a^{-1}}$ (see, e.g. Lee et al., 1998; Joos et al., 1999; Le Quére et al., 2000) but is currently under debate (Thomas et al., 2001). The Southern Ocean is such a major high latitude area and plays a crucial role in the global carbon budget both for gross (natural and anthropogenic) as well as net (anthropogenic only) exchanges of CO_2 with the atmosphere (Hoppema et al., 1999; Caldeira and Duffy, 2000). In this area the upwelling of deep waters rich in dissolved CO_2 and major nutrients tends to cause overall CO_2 outgassing. However, the drawdown of CO_2 by phytoplankton blooms offsets this outgassing, and the overall Southern Ocean may well be a gross sink rather than a source of atmospheric CO_2 (Louanchi et al., 1999). In addition the formation of Antarctic intermediate water (AAIW) and Antarctic bottom water (AABW) transfers dissolved CO_2 into the deep ocean (Anderson and Jones, 1991). Similarly there is significant net uptake of anthropogenic CO_2 which eventually appears to be transported into other deep ocean basins (Caldeira and Duffy, 2000; Thomas and England, 2002).

A compilation of surface water partial pressure of CO_2 (pCO_2) data by Takahashi et al. (1993, 1997) suggested that a temperature component is largely responsible for the observed pCO_2 distribution. Recent work in Antarctic waters confirmed the effect of temperature, but plankton blooms were shown to be more important (Bakker et al., 1997; Hoppema et al., 1995). These blooms are probably regulated by the availability of light and iron (de Baar et al., 1995), since major nutrients are in abundant supply by the upwelling in this so-called high nutrient–low chlorophyll area (de Baar and Boyd, 2000). In this paper we demonstrate the impact of marginal ice zone (MIZ) phytoplankton blooms on the uptake of CO_2 from the atmosphere. High-resolution online surface water measurements of the carbonate system in four longitudinal transects are combined with distributions of Chl$a$ and hydrographic variables in our analysis. Finally, an attempt is made to quantify the roles of biology and physics with a simplified mass balance model.

2. Sampling and methods

Data are presented from cruise ANTXIII/2 aboard R.V. "*Polarstern*" from 4 December 1995 to 24 January 1996 (austral summer; Bathmann et al., 1997a). Meteorological and underway data were obtained from the ship's data-acquisition system. Two long transects (Fig. 1) were made, each consisting of two legs (1A and 1B, 2A and 2B; see Table 1) between (but not crossing) the Polar Front and Antarctic Continent. During these transects continuous underway measurements were made of total carbon dioxide content (TCO_2), the fugacity of CO_2 and the major nutrients as well as temperature and salinity.

The sum of all inorganic carbonate species in seawater, collectively known as TCO_2, was determined by a high precision Coulometric titration (Stoll et al., 1993). Although the method is commonly used for analysis of discrete water samples (Johnson et al., 1987) underway measurements can also be performed (Robinson and Williams, 1992), and it is the latter that are reported here. Seawater was pumped from 8 m depth and fed through the automated extraction line. An accurate volume of subsample was taken once every 5 min and acidified with phosphoric acid (8.5%) and stripped with high purity nitrogen gas. The carrier gas together with the CO_2 gas was led through a cell containing a solution of ethanolamine and an indicator. The solution was electrochemically backtitrated to its original colour, and the total amount of Coulombs used was employed to calculate the moles of CO_2 titrated. Standardization was obtained by regular measurements of a certified TCO_2 standard (DOE, 1994; pooled $STD \pm 2.1\,\mu\mathrm{mol\,kg^{-1}}$) made available by Dr. A. Dickson (SCO, USA). The data were post-processed and screened for obvious outliers, resulting in a dataset totaling over 3200 datapoints.

The fugacity of CO_2 in air and in seawater was measured with a home-built extraction unit/analyzer (designed after Wanninkhof and
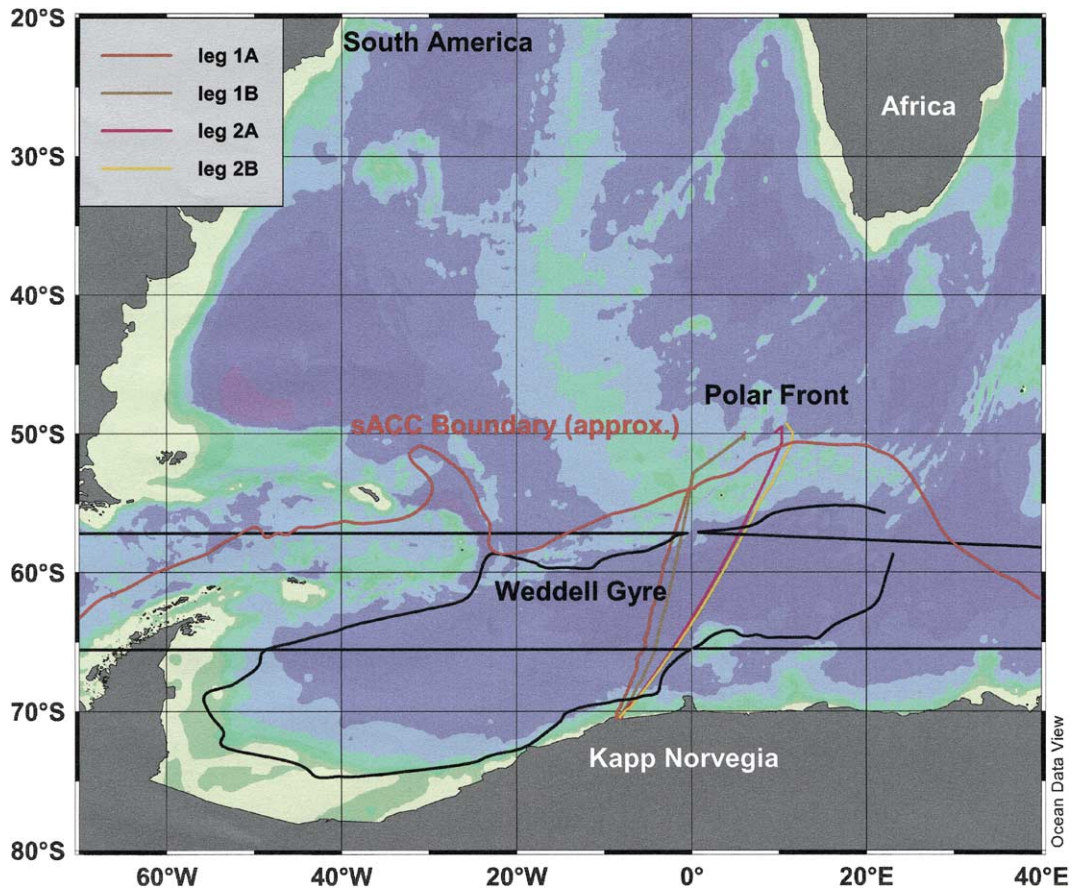
Fig. 1. Map showing the study area. Approximate locations of the Polar Front and the WG circulation are shown, transect 1 (legs 1A and 1B) and transect 2 (legs 2A and 2B) by the solid lines. The three different hydrographic regions have been indicated (sACC = southern Antarctic Circumpolar Current).

Table 1
Starting and ending dates of the four transects from the Polar Front $\sim 50°N$, 11°E) to camp Neumayer ($\sim 68.5°N$, 7°W)

Transect no.	Leg	Start date	End date
1	1A	09-12-1995	15-12-1995
	1B	19-12-1995	24-12-1995
2	2A	06-01-1996	11-01-1996
	2B	15-01-1996	19-01-1996

Thoning, 1993) including a Li-Cor (LI-COR, Model 6252) infrared analyzer. Marine air was pumped from the crow's nest into the ship laboratory through Dekabon tubing, which was flushed continuously until a subsample was taken.

The same seawater supply as used for the TCO_2 determination was used for measurements of fCO_2 in seawater with a modified equilibrator after the design of Watson (*see also* Bakker et al., 1997; their Fig. 3). At a rate of approximately $40–60 \, cm^3 \, s^{-1}$ the seawater is sprayed through a showerhead into the equilibration chamber. The system has a response time of less than 2 min. A vent connected to marine air supply maintained atmospheric pressure, thereby avoiding contamination of the headspace gas. The temperature of the seawater in the equilibrator and in the outflow was continuously logged with calibrated Pt-100 resistance thermometers and later coupled with the

shipboard meteorological data (England, 1997). Both seawater and air samples were dried with Aquasorb (Merck) before being passed through the IR analyzer. Because CO_2 in air is a non-ideal gas mixture (Weiss, 1974) we use the appropriate property fugacity of CO_2 (fCO_2 in µatm) rather than the partial pressure of CO_2 (pCO_2 in ppm), although the difference is rather trivial, being on the order of 0.7%.

The fCO_2 system was calibrated with reference gases, which in turn had been calibrated versus National Oceanic and Atmospheric Administration (NOAA) certified standard gas mixtures (accurate to 0.01 ppm), before and after the cruise. For all reference gases the precision during the calibration was better than 0.07 ppm. No significant difference could be observed between the pre-cruise and post-cruise calibrations. A typical analysis cycle (which takes less than 1 h) consists of a calibration with three reference gases, air, seawater ($5 \times$), air, seawater ($5 \times$) and a calibration. For each sample 10 readings were taken and averaged during post-processing. Final data were obtained by interpolation between two consecutive calibration cycles.

Because of the transport of water from the ship inlet to the equilibrator, a slight warming occurred, in extreme cases up to 0.7 K but generally less than 0.1 K. Datapoints that were obvious outliers or had too large a temperature difference, indicating a blockage in the water supply, were deleted from the dataset. The remaining data were corrected for the temperature difference following the polynomial given by Copin-Montégut (1989). For the flux computations the shipboard meteorological data (England, 1997) and the assumption of 100% atmospheric moisture content at the sea surface were used. The flux (F in $mmol\,m^{-2}\,d^{-1}$) across the air–sea interface is given by the equation

$$F = k\,\Delta fCO_2 \tag{1}$$

in which fCO_2 is the fugacity of CO_2, k is the transfer coefficient (Wanninkhof, 1992), and ΔfCO_2 is the gradient between air and the sea surface. The transfer coefficient k is

parameterized as

$$k = [2.5(0.5246 + 1.6256 \times 10^{-2}T + 4.9946 \times 10^{-4}T^2) + 0.31u^2](Sc/660)^{-1/2} \tag{2}$$

after Wanninkhof (1992), in which T is the temperature (°C), u is the windspeed at 10 m above sea level ($m\,s^{-1}$), and Sc is the Schmidt number, a dimensionless ratio of momentum transfer and mass transfer. The coefficient includes also the role of chemical enhancement of CO_2 gas transfer at low windspeeds (Wanninkhof, 1992).

Samples for nutrient determination were taken every half hour and measured on a Technicon Autoanalyser II system (Hartmann et al., 1997). The data were also coupled to the carbonate dataset. To facilitate all further computations, data were linearly interpolated over the shortest section length, thus resulting in an equidistant dataset. Table 1 lists the start and end dates of the four sections.

Based on the ship data for windspeed, the wind mixed layer (WML) depth was computed as a first approximation. WML was taken as being half of the computed Ekman depth ($= 2.5$ times the average windspeed at 10 m height; see also Veth, 1991) under the assumption of instantaneous mixing. Fluorescence data were also obtained from the ship data, and expressed as chlorophyll *a*, following the method described by Bathmann et al. (1997b).

3. Results

3.1. Hydrography

The study area is situated in the Antarctic Circumpolar Current (ACC) and in the subpolar region, where it includes both the eastward and westward flowing limbs of the Weddell Gyre (WG) (*see* Fig. 1). In view of the fact that only surface measurements were made, the hydrography is simplified to having only Polar Front Surface Water (PFSW) and Antarctic Surface Water (ASW). A number of fronts exist in this region and have been described in detail (e.g. Orsi et al., 1995; Belkin and Gordon, 1996; Veth et al., 1997).

Based on literature and the real-time data, a distinction could be made between three different regions for our study area (which is between 50°S and 70°S). The WG area stretches from 56°S to 70°S and the ACC from 50°S to 56°S. Around 56°S latitude, also known as the ACC–WG boundary, a more detailed division of the ACC is made into two regions; the southern Polar Front (sPF) and the southern Antarctic Circumpolar Current (sACC; see Table 2; Veth et al., 1997).

Distributions of temperature and salinity in the transects are given in Fig. 2. Over the whole of Transect 1 (Figs. 2a) salinity ranged from 33.8 to 34.35. For both legs 1A and 1B, the values in the north are lower than in the south near the continent. Temperature ranged from 4.2°C in the

Table 2
Hydrographic regions for the four legs (1A and 1B; 2A and 2B), as defined for the study area

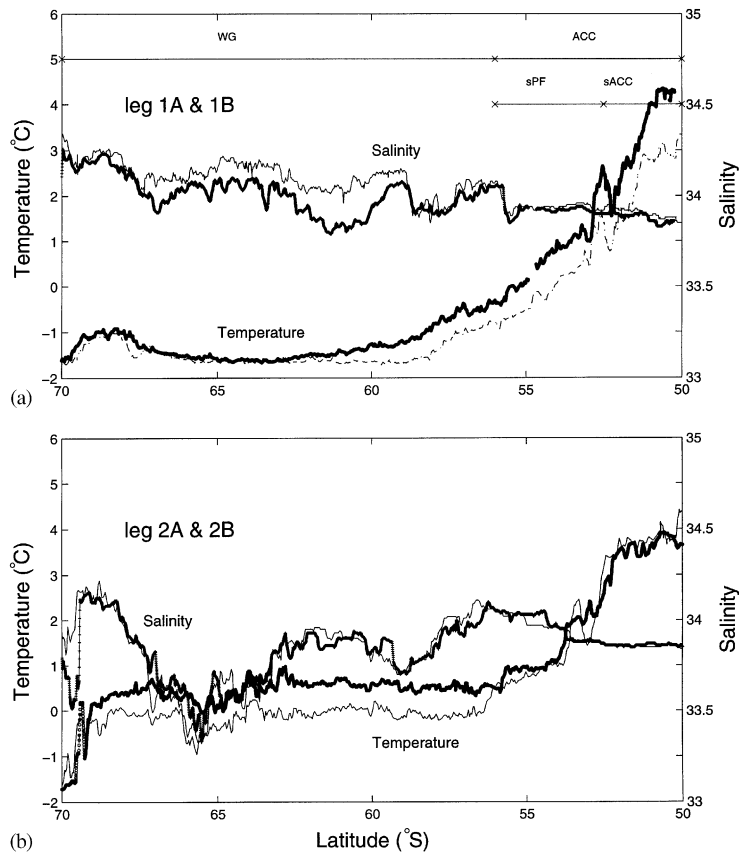| Hydrographic region	Abbreviation	Latitude (°S)
Southern ACC	sACC	50 ≤ ACC < 52.5
Southern Polar Front	sPF	52.5 ≤ sPF < 56
Antarctic Circumpolar Current	ACC	50 ≤ ACC < 56
Weddell Gyre	WG	56 ≤ WG ≤ 70

Fig. 2. Plots of temperature/salinity sections of the surface waters of both transects. (a) Legs 1A and 1B of transect 1, (b) legs 2A and 2B of transect 2. Thinner lines are the legs southward and the bold lines northward. In the upper two figures the different hydrographic regions are shown by lines. ACC = Antarctic Circumpolar Current divided into the sACC (= southern Antarctic Circumpolar Current) and the sPF (= southern Polar Front); (WG = Weddell Gyre).

north to $-1.8°C$ (freezing point) in the south. A gradual decrease is seen southward to nearly constant values ($\sim -1°C$ to $-1.5°C$) except for somewhat higher values near the coastline. The return leg 1B showed a local increase near $50°S$ of $\sim 1°C$ that occurred in 9 d. On Transect 2 the salinity ranged from 33.25 to 34.25, in the north approximately 33.65 (Figs. 2b). The same pattern is observed for both legs 2A and 2B, where salinity minima are observed at $65°S$ and near the coastline, probably due to the influence of meltwater. Except for near the coastline and near the Polar Front, temperature increased slightly ($\sim 0.5°C$) in the timespan of 15 d between legs 2A and 2B. The nearshore areas actually showed a slight decrease in temperature. Both the transects exhibit a sharp change in temperature in the area of 52–$53°S$.

3.2. fCO_2

The fugacity of CO_2 in the atmosphere undulates (Figs. 3a and b and Figs. 4a and b), being directly correlated with variations in atmospheric pressure. Some gaps exist in the data, either due to absent auxiliary data (e.g. temperature or salinity) or due to erroneous fCO_2 data, which have been deleted. Leg 1A is characterized mostly by supersaturation in fCO_2 in the surface water, relative to the atmosphere (Fig. 3a). In the south supersaturations of ~ 10–$15\,\mu atm$ are observed, with near equilibrium values near $60°S$. Further north values are seen to increase again, with a slight undersaturation present at $54°S$. No clear correlation can be seen between Chl$a$ levels and the fCO_2 in the water. The return leg 1B displays pronounced undersaturation, especially north of $62°S$ (Fig. 3b), although a clear correlation with Chl$a$ could not be detected. Only near $50°S$ is a slight increase in Chl$a$ seen with a coinciding undersaturation in fCO_2.

Transect 2 (leg 2A) shows undersaturation in fCO_2 near $50°S$, which increases rapidly southward to a large supersaturation (Fig. 4a) of up to $75\,\mu atm$. Further south the supersaturation changes to undersaturation ranging from $-60\,\mu atm$ in the continental region to $-90\,\mu atm$ at $63°S$. The observed undersaturations are matched by elevated Chl$a$ levels in the range of 2–$3\,\mu g\,l^{-1}$, comparable with findings of Schneider and Morlang (1995). The return leg 2B (Fig. 4b) shows, surprisingly, a less pronounced undersaturation in fCO_2 at the southern end of the transect but very high Chl$a$ content (up to $8.6\,\mu g\,l^{-1}$ near the continent). The fCO_2 undersaturation at $64°S$ diminished in a few days to a value of $-40\,\mu atm$ because of the increase in WML (Figueiras et al., 1994) even though the Chl$a$ remained approximately the same. Near the Polar Front the large supersaturation decreased in a timespan of 15 d to near equilibrium values with a slightly increased Chl$a$ content. Silicate increased in the time period between legs 2A and 2B in this region.

3.3. Chlorophyll a, plankton and nutrients

Comparing the major nutrients silicate and nitrate for both legs 1A and 1B (Figs. 3c and d) one can observe only near the Polar Front a decrease in both nutrients. Silicate decreased by $\sim 5\,\mu mol\,kg^{-1}$ and nitrate by about $2\,\mu mol\,kg^{-1}$ over the 9-d period between the two legs. For both the legs both nitrate and silicate appear to be relatively constant from the continent to approximately $55°S$. From here a rapid decrease with decreasing latitude is seen. This gradient did not change over time. In the region between $60°S$ and $70°S$ the largest undersaturations in fCO_2 were observed, thus justifying a closer look. Transect 1 (with its relatively low Chl$a$ levels) shows for both legs a nearly constant Si/NO_3 ratio of ~ 2.4, which increases near the continent to about 2.8, coinciding with an increase in Chl$a$. These observed increases of the ratio indicate the growth of non-diatom species (e.g. *Phaeocystis*). Very close to the continent the ratio drops sharply to a value of ~ 2.2. The return leg depicts a similar pattern, but very near the continent the ratio has increased from 2.2 to 2.4 in a few days.

The more eastern transect 2 (Figs. 4c and d) had much higher Chl$a$ levels (Figs. 4a and b). The Si/NO_3 ratios start at 0.4 near the Polar Front and increase rapidly to ~ 2.4 near the southern Polar Front. They decreased to ~ 2.0 at $62°S$ during leg
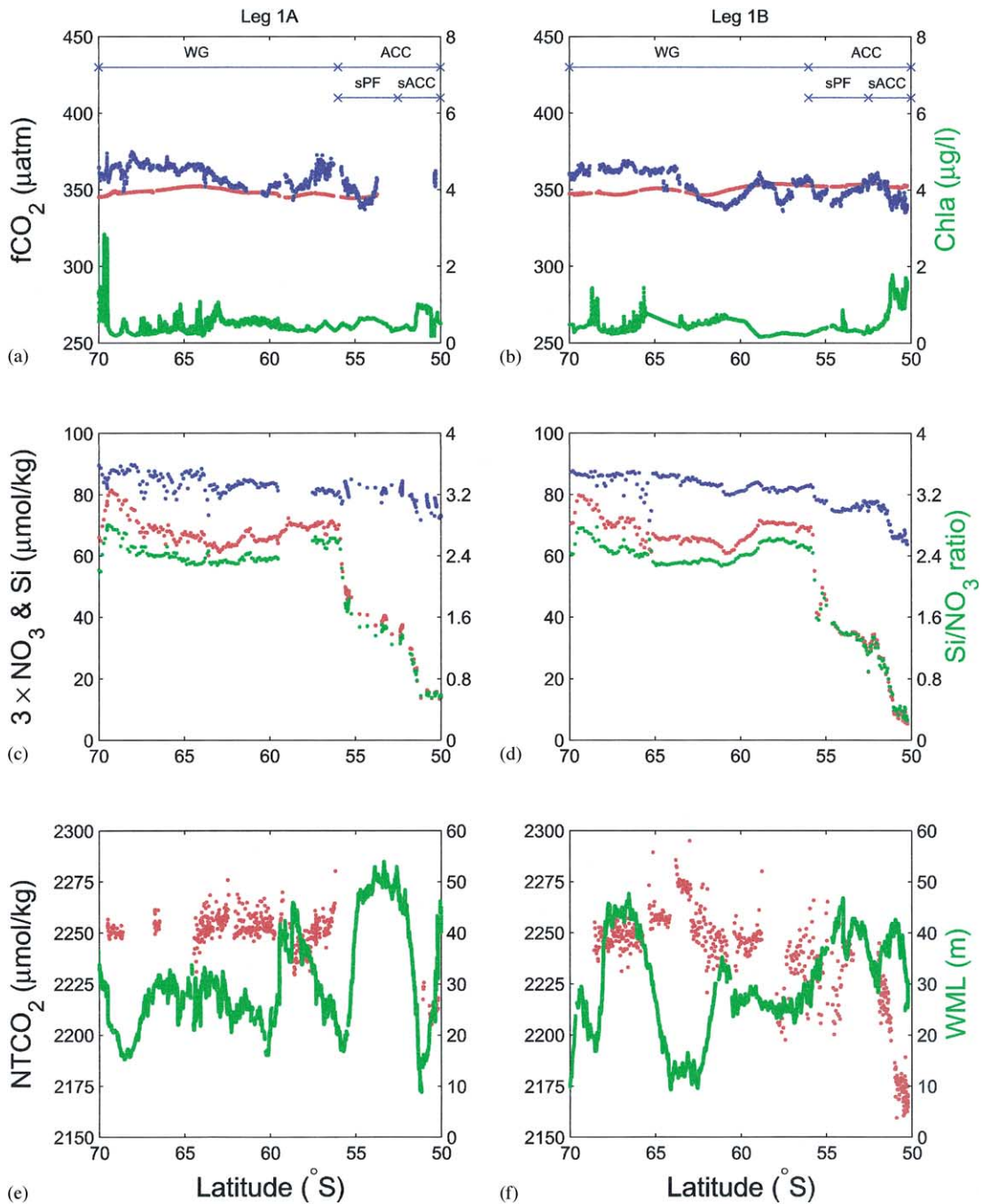
Fig. 3. Plots for legs 1A and 1B of: (a,b) the fugacity of CO_2 in air (red) and water (blue) (both in µatm) and Chl$a$ (in µg/l), (c,d) silicate (red) and NO_3 ($\times 3$; blue) (in µmol kg^{-1}) and the Si/NO_3 ratio (green), (e,f) normalized TCO_2 ($NTCO_2$ versus a salinity of 35 in µmol kg^{-1}) and the WML (m).
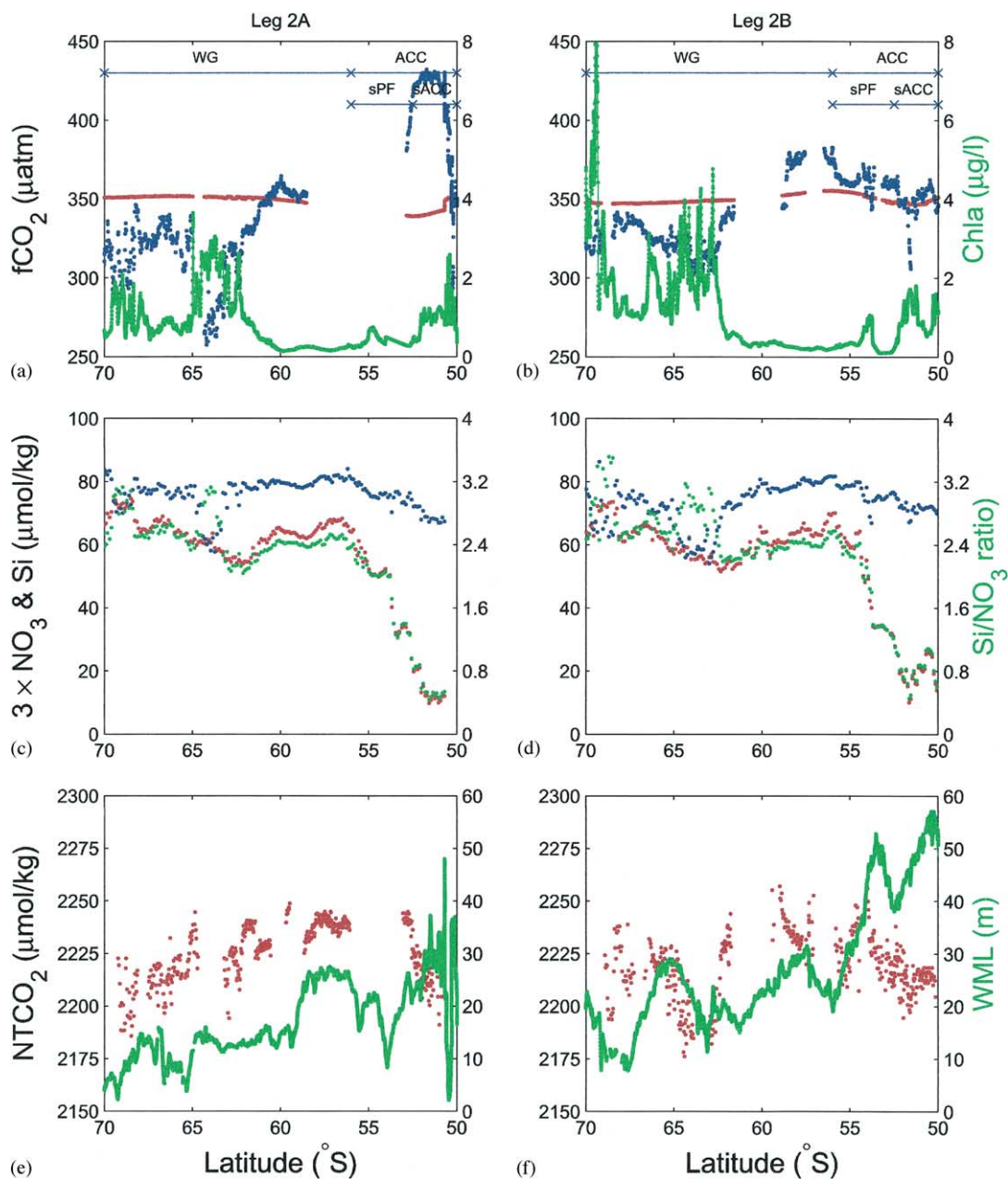
Fig. 4. Plots for legs 2A and 2B of (a,b) the fugacity of CO_2 in air (red) and water (blue) (both in μatm) and Chl*a* (in μg/l), (c,d) silicate (red) and NO_3 (×3; blue) (in μmol kg^{-1}) and the Si/NO_3 ratio (green), (e,f) normalized TCO_2 ($NTCO_2$ versus a salinity of 35 in μmol kg^{-1}) and the WML (m).

2A. From here high ratios are observed coincident with high Chl*a* levels consistent with blooms of *Phaeocystis* (Bathmann et al., 1997a, b) rather than diatoms. Further south the ratio decreases again to about 2.4 and is at the maximum near the continent. The low ratios next to the continent are

again indicative of preceding or active diatom blooms. The return leg 2B shows a similar pattern although, the ratios have increased, as have the Chl$a$ levels. The very low ratio of 2.0 at 62°S present on leg 2A has now increased to a value of 2.4.

3.4. TCO_2

TCO_2 data were normalized ($NTCO_2$) to a salinity of 35 to exclude freshwater influence and are shown in Figs. 3e and f and Figs. 4e and f. Legs 1A and 1B have values ranging from as low as 2159 µmol kg^{-1} near the Polar Front (Figs. 3e and f) up to ∼2290 µmol kg^{-1}. Especially near the Polar Front a clear decrease (up to ∼50 µmol kg^{-1}) in $NTCO_2$ is observed, which is probably caused by a different watermass rather than by biological uptake, given the only slight increase in Chl$a$ content. Only temperature increased, by ∼1°C; the salinity stayed constant (Fig. 2a). Figs. 3c and d, however, show a change in silicate and nitrate supporting the option of a different watermass. Such a large decrease in $NTCO_2$ cannot be explained otherwise. The southward bound leg of Transect 2 (leg 2A) shows $NTCO_2$ values ranging from 2185 to 2250 µmol kg^{-1}. Low values are seen near the Polar Front and near the continent showing some, albeit small, correlation with the Chl$a$ signal. The return leg (leg 2B) depicts a similar pattern (values ranging from 2175 to 2255 µmol kg^{-1}) with a large dip seen at ∼64°S, which indeed matches the higher Chl$a$ content. No correlation between $NTCO_2$ and temperature (Figs. 2c and d) could be found.

3.5. Air–sea CO_2 exchange

Fluxes of CO_2 across the air–sea interface were calculated from in situ values of the meteorological parameters, notably wind velocity (Wanninkhof et al., 1992; Bakker et al., 1997).

Leg 1A shows negative fluxes (Fig. 5a) (i.e., outgassing to the atmosphere and thus a decrease of surface water TCO_2) along the whole transect, except for a very slight positive flux (i.e. uptake) at ∼58°S. Such general outgassing is consistent with

either continuous upwelling of older CO_2-rich deep waters, or seasonal warming of surface waters, or the combination of both processes. The return leg, 1B, shows outgassing in the WG area (Fig. 5b) and a very high flux to the atmosphere near 67°S, due to a very high windspeed at this position. The flux changes sign at approximately 62°S, and continuing northward CO_2 is taken up by the surface waters. The ACC region has changed in this time period from a source to a sink for CO_2. In this season, when water temperatures are still increasing, such ocean uptake can be ascribed only to biological fixation of CO_2, more than offsetting the outgassing force due to upwelling or seasonal warming.

Leg 2A shows a positive flux from the continent to ∼61°S (Fig. 5c). This part of WG is, in contrast to what was observed on the more western transect 1 (legs 1A & 1B), a sink instead of a source. The sACC area, with the observed strong supersaturation during leg 2A (Fig. 4a), releases CO_2 to the atmosphere. On the return leg 2B, the air–sea gradient has decreased with an undersaturation here and there (Fig. 4b). Because of the increase in WML depth (Figs. 4e and f), the flux has increased though (Fig. 5b). The WG shows a parallel behaviour, from strong undersaturation (leg 2A) to a lesser undersaturation (leg 2B; Figs. 4a and b). The flux has increased, also because of the increase in WML depth, and the area, which is a sink, has extended to ∼58°S in approximately 6 d (Fig. 5d). From this latitude northward the flux is generally negative, i.e., CO_2 is released to the atmosphere.

Fig. 5e shows the mean flux for the three different regions during legs 1A and 1B of transect 1. The WG area is a source during both legs, but the mean flux is halved (from ∼4 to ∼2 mmol m^{-2} d^{-1}) in a time period of ∼6 d. Both the sPF and the sACC regions changed from source to a sink in a period of 9 d. The sPF has nearly the same magnitude, whereas the sACC region has an almost two-fold higher value. Transect 2 (Fig. 5f) shows the WG region to be a slight sink on the order of ∼−1 mmol m^{-2} d^{-1}. In 6 d this value nearly tripled to ∼−2.5 mmol m^{-2} d^{-1}. This change can be attributed to an increased wind velocity rather than to

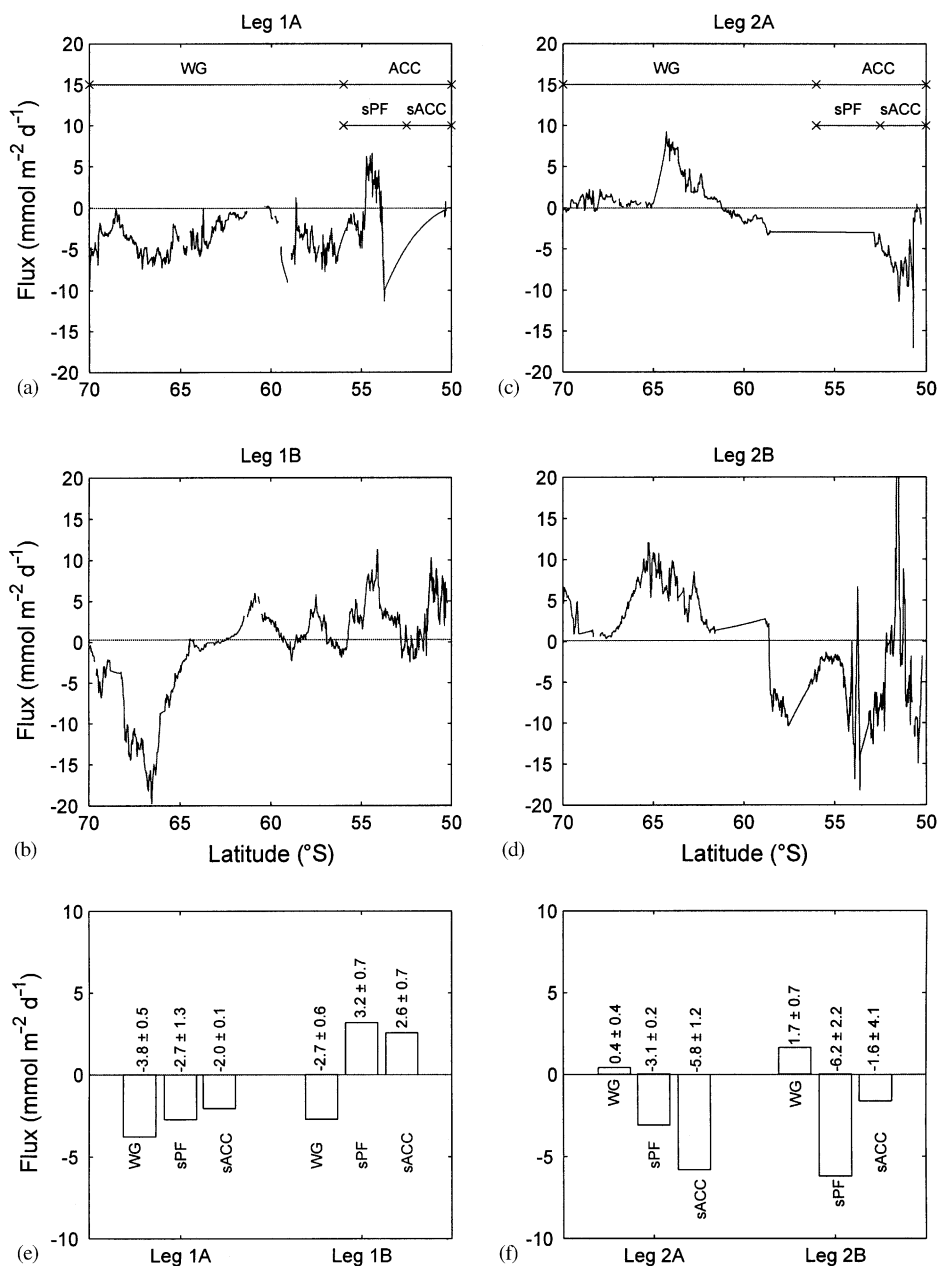Fig. 5. Realtime CO_2 flux (in mmol m^{-2} d^{-1}) for all four legs: (a) leg 1A, (b) leg 1B, (c) leg 2A and (d) leg 2B. In the lowest two plots the mean flux per hydrographic region (e) transect 1 and (f) transect 2. Positive fluxes are into the sea, negative fluxes out of the sea.

an increased CO_2 gradient. The sPF region has increased the mean source value from 4 to about 5 mmol m^{-2} d^{-1}. The sACC region has on leg 2A a strong mean source value of ~ 7.5 mmol m^{-2} d^{-1}

and on leg 2B (9 d later) a value of about 4 mmol m^{-2} d^{-1}. The lower value is the result of occasional undersaturation (negative flux), thus diminishing the mean value for overall outgassing.

4. Discussion

4.1. Phytoplankton growth and undersaturation of fCO_2

Physical processes that affect fCO_2 are horizontal and vertical advection, dispersion and initial state of the watermasses, the depth of the WML, and air–sea gas and heat exchange. As evident from Figs. 3e–f and Figs. 4e–f, the depth of the WML near the Polar Front is variable but on average around 30–40 m deep. Near the continent the WML tends to be rather shallow (about 10–15 m) for leg 1B and both legs of transect 2 (leg 2A & 2B). Part of the shallow WML during leg 1B may be attributed to the larger ice coverage (van den Brink and van Franeker, 1997, their Fig. 2.2), but observations showed no complete coverage and only a few places where coverage was more than 80%. Although the ice coverage was even stronger on leg 1A, a clear correlation between the depth of the WML and ice coverage cannot be found. Transect 2 showed negligible ice cover.

The observed increase in temperature (~ 1 K) near the Polar Front corresponds to a potential increase in fCO_2 of about 14 µatm (Bakker et al., 1997). The fCO_2 did not increase though, but decreased in combination with a slight increase in Chl$a$. The undersaturation near the Polar Front is thus probably due to the combined effect of phytoplankton growth and the advection of water with a lower TCO_2 content. We assume alkalinity to be conservative in the Antarctic Ocean (Anderson et al., 1991; Stoll et al., 1999) as the nitrate effect of photosynthesis on alkalinity is deemed to be of minor importance. Thus a lower TCO_2 would result in a lower fCO_2. For transect 2 the temperature increased by ~ 0.4 K in time between the two legs. The observed change in temperature increases the fCO_2 by about 5 µatm, thus lowering the observed undersaturation gradient by about 5%. The remainder is then due to phytoplankton growth, and the relation with fCO_2 undersaturation is still clearly visible. It is interesting to note that high Chl$a$ abundance does not mean the largest undersaturation. The flux across the air–sea interface is rather small because of low windspeed and thus not able to compensate completely for large undersaturations. It is more likely that the onset of phytoplankton growth with their strong uptake of CO_2 results in the observed gradient of fCO_2. The resultant biomass increase is then seen on the return leg 2B, in which the system shows less undersaturation. The latter effect is ascribed to an influx of CO_2 from the atmosphere and less productive (smaller growth rate = smaller CO_2-uptake) phytoplankton.

In order to deduce which group of phytoplankton is responsible for the observed phenomena we plotted the silicate–nitrate ratios (Figs. 3c and d and Figs. 4c and d). During growth, uptake of nitrate and, in the case of diatoms, also silicate takes place. Transect 1 does not show a clear ratio change except near the continent on leg 1A (Figs. 3c and d). There the ambient decrease in the Si/NO_3 ratio suggests an increase in the diatom population. On transect 2 (Figs. 4c and d) the Si/NO_3 ratio increases by ~ 40–60% thus indicating that not diatoms but other algae are the dominant group of phytoplankton. This is also supported by data from Bracher et al. (1999), which indicate that at some stations sampled at the transects some 20–40% of the phytoplankton are diatoms, the remainder being a combination of non-silicon-containing dinoflagellates, prymnesiophytes and chrysophytes.

Our approach to calculate the mean fluxes per region has the drawback that it is based on a latitudinal section. In order to assess the effects of different processes (seasonal warming, upwelling, biological fixation, respiration) one ideally needs a time series (Bakker et al., 1997). In this way one would have the initial state and the evolution in time, enabling quantification of the above-mentioned processes. Our four individual latitudinal sections merely are snapshots in time. However, the combination of both legs of one transect can give us an initial state and a later stage. Thus, we were able to develop a simple budget model to identify the cause of the observed changes in the carbonate system.

4.2. A simple budget model

The observed changes in TCO_2 and fCO_2 in the water, an upwelling term (Ekman pumping), an

eddy-diffusive flux and net community respiration (ΔB) (Hansell and Carlson, 1998) are incorporated in the simple model described below (see Fig. 6). Other terms are mixing of water masses and the initial state of these water masses, of which the latter is ignored in this work. Our purpose is to quantify the role of biology in the carbon transfer in the system in combination with physical processes. Time series of one water mass is ideal for this kind of work. Here the online surface water measurements between two consecutive legs of one transect (1A versus 1B; 2A versus 2B) are taken as an approximation. Both transects (1 and 2) started at the Polar Front (legs 1A & 2A), and their return legs (legs 1B & 2B) end at the Polar Front; thus the time passed between two samplings at a given latitude must be taken into account to deconvolute the processes. Data were corrected for this time difference by dividing the observed change in the appropriate property by the number of days passed. The mixing of water masses can be accounted for by normalizing the initial property, TCO_2, to a salinity of 35. Thus the mass balance of a box of surface water (Fig. 6) (integrated over the
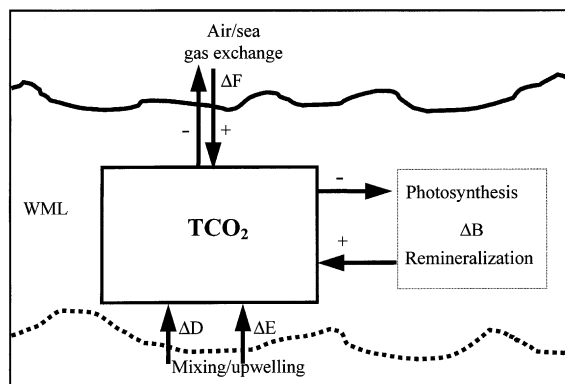
WML depth for an area of $1\,\text{m}^2$) is described by

$$\Delta C = (\Delta D + \Delta E) + \Delta F + \Delta B \tag{3}$$

in which ΔC is the observed change in TCO_2, ΔD the eddy-diffusive flux from underlying waters, ΔE the Ekman pumping term (advective flux), ΔF the atmospheric influx of CO_2 from air to sea and ΔB the closing term representing the apparent influence (respiration–photosynthesis) of biology needed to balance the budget (all in mmol $\text{m}^{-2}\,\text{d}^{-1}$). Note that positive fluxes increase the TCO_2 of the surface water box, whereas negative fluxes decrease it. This means, positive ΔB values could be seen as net community respiration and negative ΔB values as net community production, respectively.

The change in TCO_2 is described by the time-corrected change in TCO_2 integrated over the computed WML, in the formula

$$\Delta C = (C_1 - C_0) \times \text{WML} \tag{4}$$

with C_1 and C_0 the concentrations ($\mu\text{mol dm}^{-3}$) at times 1 and 0 and WML (m) the depth of the wind mixed layer. The CO_2 air to sea flux ΔF is based upon the concentration differences of CO_2 in air and the sea surface water ($\Delta p CO_2$) and is computed according to Bakker et al. (1997), Stoll et al. (1999), Wanninkhof (1992) and Wanninkhof and Thoning (1993). The upward terms $\Delta D + \Delta E$ describe the eddy-diffusive flux and Ekman upwelling and are taken from de Baar et al. (1995) following

$$\Delta D + \Delta E = K_Z(\partial TCO_2/\partial z) + V_u \Delta C \tag{5}$$

with K_Z being the turbulent eddy diffusivity (de Baar et al., 1995; set constant at $3.5 \times 10^{-5}\,\text{m}^{-2}\,\text{s}^{-1}$); ∂TCO_2 (and ΔC) the difference in TCO_2 concentration between surface water and deeper layers (on average $25\,\mu\text{mol kg}^{-1}$; based on field data) and ∂z the thickness of the corresponding boundary layer. The upwelling velocity V_u is taken as $0.15 \times 10^{-5}\,\text{m s}^{-1}$ (taken from de Baar et al., 1995).

In view of the relatively large differences between transects 1 and 2, not only hydrographically (Fig. 2) but also topographically (Fig. 1), a budget per transect is made. If the two transects had been more closely related, one could also have

Fig. 6. The illustration represents the terms in Eq. (3) of the text. An increase of the TCO_2 inventory of the surface layer box (ΔC) can be due to the influx of CO_2 (ΔF), due to eddy-diffusive influx from the underlying water layers (ΔD) with higher TCO_2 concentrations, due to upwelling from the same layers (ΔE) or due to net biological respiration (ΔB). Reverse processes ΔF (CO_2 efflux to the atmosphere) and ΔB (net biological production) would correspond to a negative ΔC, i.e., a decrease of the TCO_2 inventory of the surface layer box. WML denotes the wind mixed layer depth of the surface box.

looked at time-related differences between transects 1 and 2. However, the observed temperature/salinity profiles differed too much to warrant this approach.

Fig. 7 shows the time-corrected plots for the various terms of Eq. (3) of the two transects. Sections were subtracted from one another in order to arrive at net changes per day (corrected for elapsed time between samplings). Figs. 7a–e and g show the results for transect 1. The ΔC is seen (Fig. 7a) to increase sharply from about 3 to a

value of about $9 \, \text{mmol m}^{-2} \, \text{d}^{-1}$ in the WG region (68°S). From here northward a rapid decrease is seen to a value of about $-5 \, \text{mmol m}^{-2} \, \text{d}^{-1}$ at 63°S. Further north ΔC alternates from positive to negative, ending at about $0 \, \text{mmol m}^{-2} \, \text{d}^{-1}$ in the Polar Front. The air–sea flux term ΔF is positive only between 66° and 68°S and remains mostly negative (on average $\sim -0.5 \, \text{mmol m}^{-2} \, \text{d}^{-1}$) further north (Fig. 7c). The sums of both the eddy diffusion term (ΔD) and the Ekman upwelling term (ΔE) (Fig. 7e) are continuously positive but
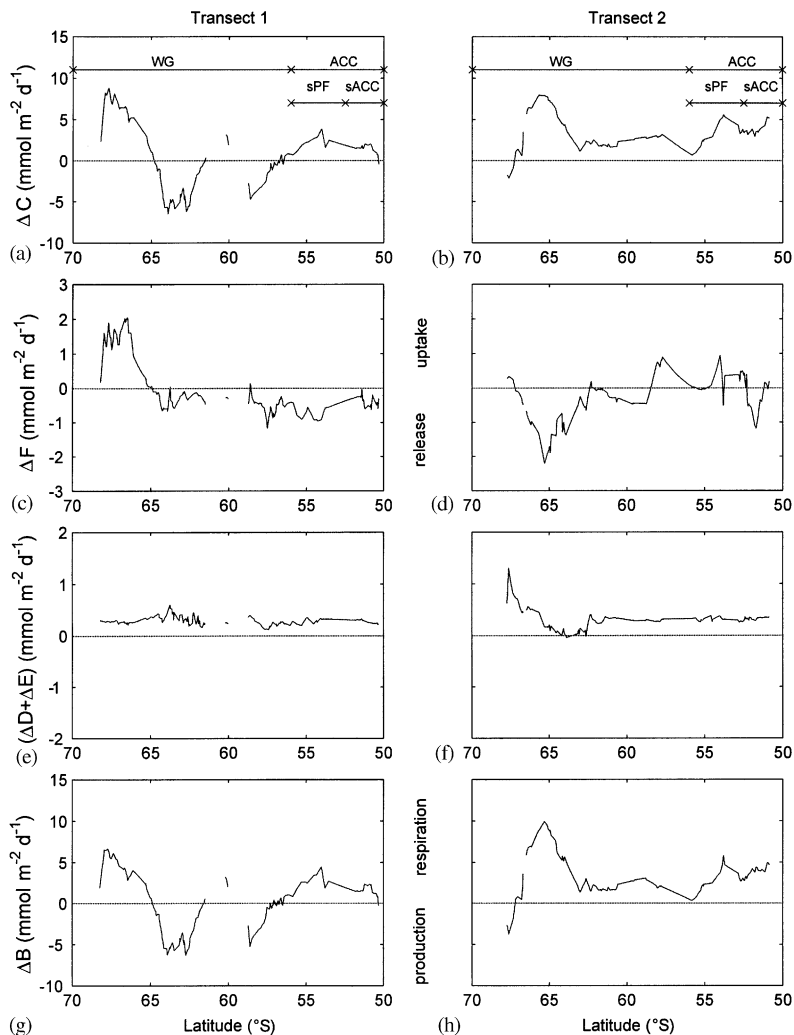

Fig. 7. The different terms of the mass balance model (Eq. (3); Fig. 6) plotted versus latitude for transect 1 (a, c, e and g) and transect 2 (b, d, f and h). ΔC = observed change in TCO$_2$, ΔF in/efflux of CO$_2$, ($\Delta D + \Delta E$) = summation of the eddy-diffusive flux and the Ekman upwelling and the closing term net community respiration (ΔB) needed to balance the budget (all in mmol m^{-2} d^{-1}).

small ($<0.5\,\text{mmol}\,\text{m}^{-2}\,\text{d}^{-1}$), indicating a continuous supply of carbon from deeper waters. Overall, ΔB (Fig. 7g) matches closely the observed pattern in ΔC. Near the continental margin ΔB increases from slightly below zero to about $7\,\text{mmol}\,\text{m}^{-2}\,\text{d}^{-1}$ indicating intense respiration. In contrast ΔB reaches very negative values ($-6\,\text{mmol}\,\text{m}^{-2}\,\text{d}^{-1}$) at 63–64°S consistent with photosynthesis. Further north the pattern closely matches that of ΔC, but ends at small positive values for ΔB, precisely coinciding with nearly doubled Chl$a$ levels (~51°S). This is also reflected in much lower nitrate and silicate values (Figs. 3c and d), suggesting a phytoplankton bloom that started during the preceding 2 weeks. The largest changes are actually observed in places where phytoplankton blooms start.

The budget terms of transect 2 are shown in Figs. 7b, d, f and h. The negative ΔC (at ~67.5°S) increases sharply to high positive values (more than $8\,\text{mmol}\,\text{m}^{-2}\,\text{d}^{-1}$) at 65°S and also rapidly drops again to a value of $2\,\text{mmol}\,\text{m}^{-2}\,\text{d}^{-1}$. Further north ΔC increases again to about 4–5 mmol $\text{m}^{-2}\,\text{d}^{-1}$. Here, the observed ΔF is mostly negative, this in accordance with the observed supersaturation along this northern part of the transect (Figs. 4a and b). The large negative ΔF at 52°S (Fig. 7d) is caused by the large change of supersaturation during leg 2A to undersaturation at leg 2B. The sum $\Delta D + \Delta E$ (Fig. 7f) remains positive throughout the entire transect, and is quite high near the continental region. The ΔB shows a large positive value at 65°S (Fig. 7h). The rapid increase in ΔB to about $6\,\text{mmol}\,\text{m}^{-2}\,\text{d}^{-1}$ corresponds to a large increase in ΔC, followed in the northward direction by a decrease to near zero levels and ending at about $3.4\,\text{mmol}\,\text{m}^{-2}\,\text{d}^{-1}$.

In parallel with transect 1 the computed changes on transect 2 can be explained by a combination of sustained phytoplankton blooms and physical forcing. The undersaturation ($<325\,\mu\text{atm}$) near the continent has actually weakened in a few days to values of around $340\,\mu\text{atm}$. The resultant ΔF compensates partially for the very large undersaturation ($<260\,\mu\text{atm}$) observed during leg 2A. The return leg 2B showed much smaller undersaturation in the $f\text{CO}_2$ of the surface water, in

contrast to the high supersaturation measured on leg 2A. The levels of Chl$a$ stayed approximately the same in this region, but unexpectedly nitrate (Fig. 4d) decreases. This phenomenon is not observed near the Polar Front.

The upward supply terms ($\Delta D + \Delta E$) were based on an assumed upwelling velocity (V_u) of $0.15 \times 10^{-5}\,\text{m}\,\text{s}^{-1}$ and a diffusion coefficient K_Z of $3.5 \times 10^{-5}\,\text{m}^{-2}\,\text{s}^{-1}$. These are annual mean values, which might be too high for the time of our study area. Comiso et al. (1993) showed that the ACC exhibits high upwelling velocities (0.3–$0.4\,10^{-5}\,\text{m}\,\text{s}^{-1}$) during the winter and lower velocities ($\sim0.1 \times 10^{-5}\,\text{m}\,\text{s}^{-1}$) in December/January. The latter value is lower by 33% and would thus decrease the ΔE term in our mass balance equation. Using a lower value in our budget model would only increase the importance of the other terms; i.e. biology would play an even more important role. The resultant term ΔB would increase by $\sim10\%$, but this would not affect our conclusions significantly.

The computations ignore the effect of lateral advection. This is an unknown variable, which has been implicitly taken included in the ΔB term, since no data were available to quantify lateral advection independently. However, lateral advection is deemed to be of minor importance in the timeframe observed. This assumption is supported by only low averaged eastward flows of the ACC of about $0.025\,\text{m}\,\text{s}^{-1}$ (Veth et al., 1997). The elapsed time of 15 d between legs would correspond to only 32 km, for which it might be reasonable to neglect lateral transports.

Phytoplankton blooms appear to have the potential for uptake (positive values) on the order of 6–9 mmol $\text{m}^{-2}\,\text{d}^{-1}$, which make them the major forcing factor in the drawdown of atmospheric carbon dioxide. Physical forcings (ΔF and $(\Delta D + \Delta E)$) have a large potential (values of up to $2\,\text{mmol}\,\text{m}^{-2}\,\text{d}^{-1}$ were observed), but in the time frame of our study appeared to be of relatively minor importance compared to the effects of phytoplankton blooms and respiration. Our simple mass balance model has shown that at several locations over a short time span the effects of blooms and respiration can be quantified.

4.3. Concluding discussion

Both the observed coincidences of distributions of fCO_2 and Chl$a$ (Figs. 3–4) and the calculated gas exchange fluxes (Fig. 5) demonstrate the importance of biological processes for local CO_2 exchange with the atmosphere. This is not only for uptake of CO_2 due to photosynthetic fixation, but also for outgassing due to biological respiration within the upper wind mixed layer. As a result a wide range of over- and undersaturations, with concomitant out- and influxes of CO_2, are observed (see also Takahashi et al., 1993; Bates et al., 1996; Cooper et al., 1996; Thomas and Schneider, 1999). The supersaturations also result partially from seasonal warming affecting solubility, as well as from general upwelling of CO_2-enriched deep waters.

The instantaneous air–sea fluxes (Figs. 5a–d) are quite valid, but basin-wide extrapolation in space, and more notably in time over the complete summer or full year, is difficult. The spatial extrapolation for a larger part of the ACC would appear quite reasonable, because of its fairly homogenous spatial hydrography and consistent eastward flow. Similarly our findings may well be representative for a larger part of the Weddell Gyre, if it is assumed that the general patchiness of blooms in both the Weddell Gyre and the ACC would cancel out statistically over a larger region.

Thus the mean fluxes (Figs. 5e and f) for three major parts of the sections (WG, sPF and sACC) may well be representative for the austral summer (December–January) in the larger regions. Here we found values ranging from -7 to $+3$ mmol m^{-2} d^{-1} where the straightforward summation over 40 d would lead to an overall source

function of -0.3 mmol m^{-2} d^{-1} for this summer period. This is opposite to an overall sink function of 0.3 mmol m^{-2} d^{-1} during austral spring in the same 47–60°S region, with extremes of 3.7 mmol m^{-2} d^{-1} in the Polar Front ($\sim$47–49°S) and 2.7 mmol m^{-2} d^{-1} in the ACC–Weddell Boundary (57–59°S), respectively (Bakker et al., 1997). For one section in late summer and early autumn (March–April 1996), the strong seasonal cooling at 60–70°S led to undersaturations as low as 335 μatm, compensated by supersaturations in the 50–60°S latitude band (Hoppema et al., 2000). The average flux for the latter section into the ocean is 2.5 mmol m^{-2} d^{-1}, i.e. an influx tenfold larger than the above mean fluxes in spring and summer. For winter we have no observations.

When summing up over the whole year one would find an overall very large influx as well as an overall very large efflux term, both driven as much by biological processes (photosynthesis and respiration, respectively) as by the physics of seasonal warming/cooling and upwelling. Integrating the different fluxes for each time span of the four seasons over the entire area of the Weddell Gyre, one obtains the seasonal exchange rates (Table 3). Both spring (influx) and summer (efflux) are relatively small numbers. This is in sharp contrast with the total air to sea flux for austral autumn, which is already half of the 'missing sink' of about 2.0 PgC a^{-1} (e.g. Tans et al., 1990; Francey et al., 1995), which is partially compensated for during the winter season. The estimated annual average efflux of $\sim$0.5 PgC a^{-1} from the Weddell Sea (based on the above-mentioned datasets) is of the same order as that derived by Rayner et al. (1999) (0.1±0.5 PgC a^{-1}). It is clear though that the small net annual flux, whatever its

Table 3
Seasonal uptake (positive)/release (negative) rates based on the total surface area of the Weddell Gyre (see text)

Season	Flux (mmol m^{-2} d^{-1})	Reference	Integrated rate (PgC)
Spring	+0.3	Bakker et al. (1997)	+0.14
Summer	−0.3	This paper	−0.14
Autumn	+2.5	Hoppema et al. (2000)	+1.13
Winter	NA	NA	NA

A time period of 90 days is taken to represent the season.

direction, is the small difference between large gross influx and efflux, both of which are strongly affected by biological processes.

Acknowledgements

References

Anderson, L.G., Jones, E.P., 1991. The transport of CO_2 into the Arctic and Antarctic seas: similarities and differences in the driving processes. Journal of Marine Systems 2, 81–95.

Anderson, L.G., Holby, O., Lindegren, R., Ohlson, M., 1991. The transport of anthropogenic carbondioxide into the Weddell Sea. Journal of Geophysical Research 96C, 16679–16687.

de Baar, H.J.W., de Jong, J.T.M., Bakker, D.C.E., Löscher, B.M., Veth, C., Bathmann, U.V., Smetacek, V., 1995. Importance of iron for plankton blooms and carbon dioxide drawdown in the Southern Ocean. Nature 373, 412–415.

de Baar, H.J.W., Boyd, P.W., 2000. The role of iron in plankton ecology and carbon dioxide transfer of the global oceans. In: Hanson, R.B., Ducklow, H.W., Field, J.G. (Eds.), The Dynamic Ocean Carbon Cycle: A Midterm Synthesis of the Joint Global Ocean Flux Study, IGBP Book Series, Vol. 5. Cambridge University Press, Cambridge, pp. 61–140 (Chapter 4).

Bakker, D.C.E., de Baar, H.J.W., Bathmann, U.V., 1997. Changes of carbon dioxide in surface waters during spring in the southern ocean. Deep-Sea Research II 44 (1–2), 91–127.

Bates, N.R., Michaels, A.F., Knap, A.H., 1996. Seasonal and interannual variability of oceanic carbon dioxide species at the U.S. JGOFS Bermuda Atlantic Time-series Study (BATS) site. Deep-Sea Research I 43, 347–383.

Bathmann, U.V., Lucas, M., Smetacek, V., 1997a. The expeditions ANTARKTIS XIII/1-2 of the Research Vessel POLARSTERN in 1995/1996. Berichte Zur Polarforschung, Vol. 221, 144pp.

Bathmann, U.V., Hense, I., Nacken, M., Rynearson, T., 1997b. Surface pigment concentrations. In: Bathmann, U., Lucas, M., Smetacek, V. (Eds.), Berichte Zur Polarforschung, Vol. 221, pp. 72–77.

Belkin, I.M., Gordon, A.L., 1996. Southern Ocean fronts from the Greenwich meridian to Tasmania. Journal of Geophysical Research C101, 3675–3696.

Bracher, A.U., Kroon, B.M.A., Lucas, M.I., 1999. Primary production and physiological state of phytoplankton at the Atlantic sector of the Southern Ocean. Marine Ecology Progress Series 190, 1–16.

Van den Brink, N.W., van Franeker, J.A., 1997. Sea ice observations and icebergs. In: Bathmann, U., Lucas, M., Smetacek, V. (Eds.), Berichte Zur Polarforschung, Vol. 221, pp. 12–17.

Caldeira, K., Duffy, P.B., 2000. The role of the Southern Ocean in uptake and storage of anthropogenic carbon dioxide. Science 287, 620–622.

Comiso, J.C., McClain, C.R., Sullivan, C.W., Ryan, J.P., Leonard, C.L., 1993. Coastal zone color scanner pigment concentrations in the southern ocean and relationships to geophysical surface features. Journal of Geophysical Research 98C, 2419–2452.

Cooper, D.J., Watson, A.J., Nightingale, P.D., 1996. Large decrease in ocean-surface CO_2 fugacity in response to in situ iron fertilization. Nature 383, 511–513.

Copin-Montégut, C., 1989. Corrigendum. A new formula for the effect of temperature on the partial pressure of CO_2 in seawater. Marine Chemistry 27, 143–144.

DOE, 1994. In: Dickson, A.G., Goyet, C. (Eds.), Handbook of Methods for the Analysis of the Various Parameters of the Carbon Dioxide System in Sea Water, Version 2. ORNL/CDIAC-74.

England, J., 1997. Weather. In: Bathmann, U., Lucas, M., Smetacek, V. (Eds.), Berichte Zur Polarforschung, Vol. 221, pp. 8–11.

Figueiras, et al., 1994. Light and productivity of Antarctic phytoplankton during austral summer in an ice edge region in the Weddell-Scotia Sea. Journal of Plankton Research 16, 233–253.

Francey, R.J., Tans, P.P., Allison, C.E., Enting, I.G., White, J.W.C., Trolier, M., 1995. Changes in the oceanic and terrestrial carbon uptake since 1982. Nature 373, 326–330.

Hansell, D.A., Carlson, C.A., 1998. Net community production of dissolved organic carbon. Global Biogeochemical Cycles 12 (3), 443–453.

Hartmann, C., Hollmann, B., Kattner, G., Richter, K.-U., Terbruggen, A., 1997. Nutrients, dissolved and particulate matter. In: Bathmann, U., Lucas, M., Smetacek, V. (Eds.), Berichte Zur Polarforschung, Vol. 221, pp. 44–52.

Hoppema, M., Fahrbach, E., Schröder, M., Wisotzki, A., de Baar, H.J.W., 1995. Winter–summer differences of carbon dioxide and oxygen in the Weddell Sea surface layer. Marine Chemistry 51, 177–192.

Hoppema, M., Fahrbach, E., Stoll, M.H.C., de Baar, H.J.W., 1999. Annual uptake of atmospheric CO_2 by the Weddell Sea derived from a surface layer balance, including estimations of entrainment and new production. Journal of Marine Systems 19, 219–233.

Hoppema, M., Stoll, M.H.C., de Baar, H.J.W., 2000. CO_2 in the Weddell Gyre and Antarctic Circumpolar Current: austral autumn and early winter. Marine Chemistry 72, 203–220.

IPCC, 2001. The scientific basis. In: Houghton, J.T., Ding, Y., Griggs, D.J., Noguer, M., van der Linden, P.J., Dai, X., Maskell, K., Johnson, C.A. (Eds.), Contribution of Working Group I to the Third Assessment Report of the Intergovernmental Panel on Climate Change. Cambridge University Press, Cambridge, UK; New York, NY, USA, p. 39.

Johnson, K.M., Leb. Williams, P.J., Brandström, L., Sieburth, J.McN., 1987. Coulometric total carbon dioxide analysis for marine studies: automation and calibration. Marine Chemistry 21, 117–133.

Joos, F., Meyer, R., Bruno, M., Leuenberger, M., 1999. The variability in the carbon sinks as reconstructed for the past 1000 years. Geophysical Research Letters 26, 1437–1440.

Keeling, C.D., Whorf, T.P., 1994. Atmospheric CO_2 records from sites in the SIO air sampling network. In: Boden, T.A., Kaiser, D.P., Sepanski, R.J., Stoss, F.W. (Eds.), Trends '93', A Compendium of Data on Global Change, ORNL/CDIAC-65. Oak Ridge National Laboratory, Oak Ridge, TN, USA, pp. 16–26.

Lee, K., Wanninkhof, R., Takahashi, T., Doney, S.C., Feely, R.A., 1998. Low interannual variability in recent oceanic uptake of atmospheric carbon dioxide. Nature 396, 155–159.

Le Quére, C., Orr, J.C., Monfray, P., Aumont, O., Madec, G., 2000. Interannual variability of the oceanic sink of CO_2 from 1979 through 1997. Global Biogeochemical Cycles 14(4), 1247–1265.

Louanchi, F., Hoppema, M., Bakker, D.C.E., Poisson, A., Stoll, M.H.C., de Baar, H.J.W., Schauer, B., Ruiz-Pino, D.P., Wolf-Gladrow, D., 1999. Modelled and observed sea surface fCO_2 in the Southern Ocean: a comparative study. Tellus 51B, 541–559.

Orsi, A.H., Whitworth III, T., Nowlin, Jr., W.D., 1995. On the meridional extent and fronts of the Antarctic Circumpolar Current. Deep-Sea Research I 42, 641–673.

Rayner, P.J., Enting, I.G., Francey, R.J., Langenfelds, R.L., 1999. Reconstructing the recent carbon cycle from trace gas observations. Tellus 51B, 213–232.

Robinson, C., Leb. Williams, P.J., 1992. Development and assessment of an analytical system for the accurate and continual measurement of total dissolved inorganic carbon. Marine Chemistry 34, 157–175.

Sarmiento, J.L., Orr, J.C., Siegenthaler, U., 1992. A perturbation simulation of CO_2 uptake in an ocean general circulation model. Journal of Geophysical Research 97C, 3621–3645.

Sarmiento, J.L., 1993. Atmospheric CO_2 stalled. Nature 365, 697–698.

Schneider, B., Morlang, J., 1995. Distribution of the CO_2 partial pressure in the Atlantic Ocean between Iceland and the Antarctic peninsula. Tellus 47B, 93–102.

Stoll, M.H.C., Rommets, J.W., de Baar, H.J.W., 1993. Effect of selected calculation routines and dissociation constants on the determination of total carbon dioxide in seawater. Deep-Sea Research I 40, 1307–1322.

Stoll, M.H.C., de Baar, H.J.W., Hoppema, M., Fahrbach, E., 1999. New early winter fCO_2 data reveal continuous uptake of CO_2 by the Weddell Sea. Tellus 51B, 679–687.

Tans, P.P., Fung, I.Y., Takahashi, T., 1990. Observational constraints on the global atmospheric CO_2 budget. Science 247, 1431–1438.

Takahashi, T., Olafsson, J., Goddard, J.C., Chipman, D.W., Sutherland, S.C., 1993. Seasonal variation of CO_2 and nutrients in the high-latitude surface oceans: a comparative study. Global Biogeochemical Cycles 7, 1431–1438.

Takahashi, T., Feely, R.A., Weiss, R.F., Wanninkhof, R., Chipman, D.W., Sutherland, S.C., Takahashi, T., 1997. Global air–sea flux of CO_2. An estimate based on measurements of sea–air pCO_2 difference. Proceedings of the National Academy of Science, Vol. 94, USA, pp. 8292–8299.

Thomas, H., England, M.H., 2002. The important role of warmer waters in storing anthropogenic CO_2-evidence from a comparison between CFCs and CO_2, Naturwissenschaften, 89, DOI 10.1007/s00114-002-0348-5.

Thomas, H., Schneider, B., 1999. The seasonal cycle of carbon dioxide in Baltic sea surface waters. Journal of Marine Systems 22, 53–67.

Thomas, H., England, M.H., Ittekkot, V., 2001. An off-line 3D model of anthropogenic CO_2 uptake by the oceans. Geophysical Research Letters 28 (3), 547–550.

Veth, C., 1991. The evolution of the upper water layer in the marginal ice zone, austral spring 1988, Scotia-Weddell Sea. Journal of Marine Systems 2, 451–464.

Veth, C., Peeken, I., Scharek, R., 1997. Physical anatomy of fronts and surface waters in the ACC near the 6°W meridian during austral spring 1992. Deep-Sea Research II 44 (1–2), 23–49.

Wanninkhof, R.H., 1992. Relationship between wind speed and gas exchange over the ocean. Journal of Geophysical Research 97, 7373–7382.

Wanninkhof, R.H., Thoning, K., 1993. Measurement of fugacity of CO_2 in surface water using continuous and discrete sampling methods. Marine Chemistry 44, 183–204.

Weiss, R.F., 1974. Carbon dioxide in water and seawater: the solubility of a non-ideal gas. Marine Chemistry 2, 203–205.